applied sciences

MDPI

Article

Different Experimental and Numerical Models to Analyse Emptying Processes in Pressurised Pipes with Trapped Air

Duban A. Paternina-Verona [1], Oscar E. Coronado-Hernández [1,*], Hector G. Espinoza-Román [2], Vicente S. Fuertes-Miquel [3,*] and Helena M. Ramos [4]

[1] Facultad de Ingeniería, Universidad Tecnológica de Bolívar, Cartagena 131001, Colombia; paterninad@utb.edu.co
[2] Grupo INMEDIT S.A.S., Facultad de Ingeniería, Universidad de Cartagena, Cartagena 130001, Colombia; hespinoza@grupoinmedit.com
[3] Department of Hydraulic and Environmental Engineering, Universitat Politècnica de València, 46022 Valencia, Spain
[4] Department of Civil Engineering, Architecture and Georesources, CERIS, Instituto Superior Técnico, University of Lisbon, 1049-001 Lisbon, Portugal; hramos.ist@gmail.com
* Correspondence: ocoronado@utb.edu.co (O.E.C.-H.); vfuertes@upv.es (V.S.F.-M.)

Abstract: In hydraulic engineering, some researchers have developed different mathematical and numerical tools for a better understanding of the physical interaction between water flow in pipes with trapped air during emptying processes, where they have made contributions on the use of simple and complex models in different application cases. In this article, a comparative study of different experimental and numerical models existing in the literature for the analysis of trapped air in pressurised pipelines subjected to different scenarios of emptying processes is presented, where different authors have develope, experimental, one-dimensional mathematical and complex computational fluid dynamics (CFD) models (two-dimensional and three-dimensional) to understand the level of applicability of these models in different hydraulic scenarios, from the physical and computational point of view. In general, experimental, mathematical and CFD models had maximum Reynolds numbers ranging from 2670 to 20,467, and it was possible to identify that the mathematical models offered relevant numerical information in a short simulation time on the order of seconds. However, there are restrictions to visualise some complex hydraulic and thermodynamic phenomena that CFD models are able to illustrate in detail with a numerical resolution similar to the mathematical models, and these require simulation times of hours or days. From this research, it was concluded that the knowledge of the information offered by the different models can be useful to hydraulic engineers to identify physical and numerical elements present in the air–water interaction and computational conditions necessary for the development of models that help decision-making in the field of hydraulics of pressurised pipelines.

Keywords: emptying process; mathematical model; computational fluid dynamics (CFD); numerical modelling; trapped air; pipelines

Citation: Paternina-Verona, D.A.; Coronado-Hernández, O.E.; Espinoza-Román, H.G.; Fuertes-Miquel, V.S.; Ramos, H.M. Different Experimental and Numerical Models to Analyse Emptying Processes in Pressurised Pipes with Trapped Air. *Appl. Sci.* **2023**, *13*, 7727. https://doi.org/10.3390/app13137727

Academic Editor: José António Correia

Received: 30 May 2023
Revised: 20 June 2023
Accepted: 26 June 2023
Published: 29 June 2023

1. Introduction

The physical interaction between trapped air and water in pipes has been a problem at the design and operational level [1], for which hydraulic engineers have based their technical criteria for design and operation through technical manuals [2,3]. Even so, these technical fundamentals are often not enough information to understand in detail the behaviour of air, its origin and the formation of air bubbles and air pockets inside pipes [4–6]. In this sense, different authors have focused their attention in the last years to propose models that allow a better understanding of the interaction between air and water in closed ducts; nevertheless, a physical and numerical analysis of the water phase in pipes including the effect of trapped air has been a challenge for researchers [7,8]. The

complexity to physically understand the behaviour of air trapped in water pipes is due to the physical and mechanical properties of these fluids [6]. For example: water has a density 800 times greater than the density of air. On the other hand, air is a highly compressible gas, with a ratio of 20,000:1 with respect to the compressibility of water [5].

Most of the research associated with the development of mathematical models focuses on the study of transient flows generated in filling processes with trapped air [9–13]; however, in the last decade, mathematical models have been proposed to represent the hydraulic behaviour generated during the pipe emptying process. Research has been carried out on the analysis of emptying in pipes with pressurised air, carrying out several experimental measurements, which has led to the physical understanding of hydraulic operation. Laanearu et al. [14,15] and Tijsseling et al. [16] proposed a semi-empirical model for the representation of emptying pipes which contain pressurised air, based on the laws of conservation of mass and momentum. Coronado-Hernández et al. [17], Coronado Hernández [6] and Fuertes-Miquel et al. [18] carried out a mathematical model to study the emptying process in pressurised pipes with air valves installed at the high points of the hydraulic installations, which was validated experimentally. Romero et al. [19] applied the mathematical model, developed by Coronado-Hernández et al. [17] and Fuertes-Miquel et al. [18] in large-scale hydraulic installations.

The application of Computational Fluid Dynamics (CFD) models for the study of the emptying process in pressurised pipelines has been a recent topic in the research area, in which different authors have developed two-dimensional CFD models. Besharat et al. [20] compared the results of a two-dimensional CFD model with experimental results and a mathematical model, where air pocket pressure patterns and water drainage velocity associated with an irregular pipe were analysed; on the other hand, they also analysed the impact of air return flow for different degrees of opening of drainage valves at the discharge points. Additionally, Besharat et al. [7] proposed a two-dimensional CFD model for the analysis of the emptying of a simple pipe with air entrapped inside, where subatmospheric pressure patterns of the air pocket were compared with experimental results of other authors, in addition to predicting deformations of the air–water interface during the event. Authors as Hurtado-Misal et al. [21] proposed a 2D CFD model to represent the emptying of an irregular pipe with entrapped air, where the pressure patterns of the air pocket were compared with experimentally measured data and mathematical models proposed by other authors. In addition, authors such as Paternina-Verona et al. [22,23] carried out research to study emptying processes with trapped air and air admission orifices using two-dimensional CFD models, which presented a good numerical accuracy compared to experimental results. Additionally, Paternina-Verona et al. [8,24] performed a significant contribution to the three-dimensional analysis of transient two-phase flows in emptying manoeuvres by considering the presence and absence of air admission orifices.

Numerical models such as mathematical models and CFD models play a crucial role in properly analysing the behaviour of entrained air in pipes in engineering problems, resulting in invaluable tools for the proper understanding of this complex physical interaction. However, it is the task of the development engineer to properly adjust the physical modelling conditions to the hydraulic conditions to be simulated, as this will influence an adequate representation of the problem to be solved. In that sense, the objective of this research is to present different experimental and numerical models developed by different authors for the analysis of emptying processes in pressurised pipes with trapped air, taking into account the amount of information offered by the models and the numerical modelling conditions required in their execution, where numerical and physical results were compared to identify advantages and disadvantages of using these models in problems of hydraulic engineering. Different hydraulic emptying scenarios were tested in order to analyse and compare different numerical models, such as mathematical models and 2D/3D CFD models. For this purpose, two experimental facilities were used: (i) an irregular pipe located at the hydraulics laboratory of the Instituto Superior Tecnico at Lisbon, Portugal

and (ii) a single pipe located at the hydraulics laboratory of the Universitat Politècnica de València, Valencia, Spain.

2. Numerical Modelling in Irregular Pipelines

Irregular pipelines present a similar configuration to large-scale hydraulic pipeline networks due to changes in direction and slopes in the ground [10,22,25]. During the hydraulic operations of air-entrapment in branched systems, vacuum valves for air admission are located at the most elevated points, as these are strategic areas for the placement of these devices [2]. A branched pipeline with an internal diameter of 51.4 mm, and a total length of 7300 mm was used for the numerical evaluation of the emptying processes with trapped air, as shown in Figure 1. The draining process occurs in the two branches after full opening of the ball valves 1 and 2, with internal diameters of 23 mm (see detail sin Top View). In order to generate the drainage process, the valves were fully opened simultaneously at t_m = 1.60 s. During the initial instant t = 0, a pressure transducer located at the highest point of the hydraulic system recorded the pressure oscillations of the trapped air pocket, with a frequency of 320 datapoints per second. Additionally, an Ultrasonic Doppler Velocimeter (UDV) located at the horizontal right branch measured water drainage velocity during the emptying processes with a frequency of 4 MHz, and a a Sony Camera DSC-HX200V recorded the evolution of the air–water interface to measure the water column length. In total, four (4) tests were conducted using different air pocket lengths, including, among others, an air pocket length L_{iap} = null. The initial characteristics of the different tests are shown in Table 1.

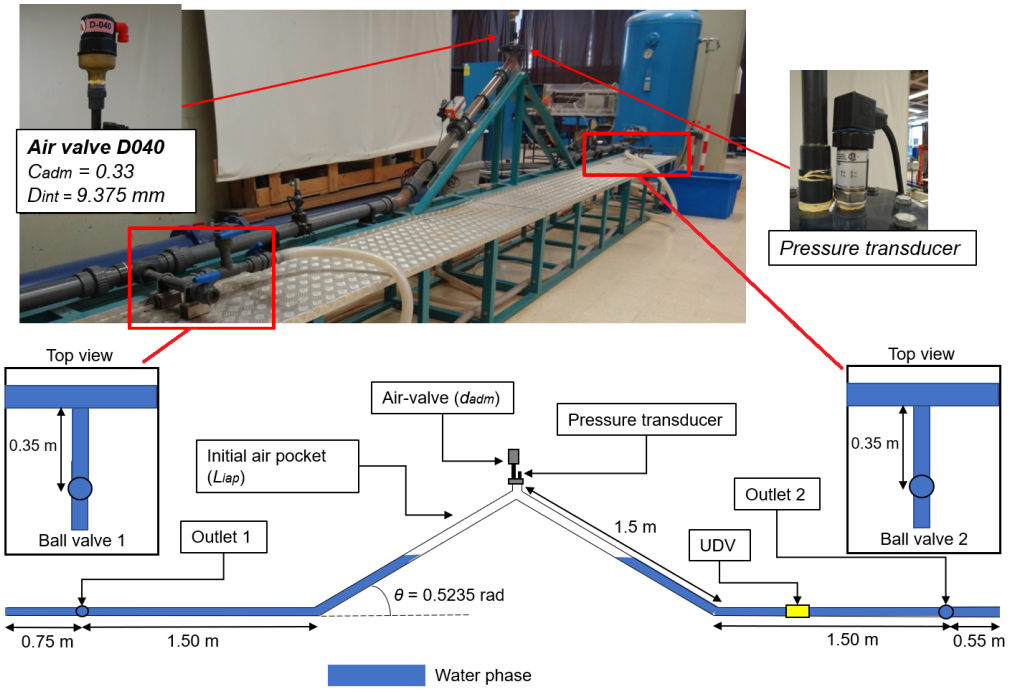

Figure 1. Experimental facility of an irregular pipeline with an air valve.

Table 1. Initial conditions of the experimental tests of the irregular pipe.

Parameter	Test 1-1	Test 1-2	Test 1-3	Test 1-4
L_{iap} (m)	null	0.54	0.92	1.32

2.1. Mathematical Modelling in Irregular Pipelines

The mathematical model for an irregular pipeline associated with the experimental installation was proposed by Coronado-Hernández et al. [17], which considers the following assumptions: (i) rigid column model considering an air–water interaction perpendicular to

the pipe axis (flow-piston model); (ii) constant inner diameter and roughness coefficient; (iii) ball valves located at the downstream end; (iv) consideration of friction losses by means of the Darcy–Weisbach equation. Since the pipeline is branched in two sections, the analysis is considered for the left branch (Emptying Column No. 1), and the right branch (Emptying Column No. 2); additionally, an air valve with cross section ($A_{adm,1}$) is considered with an admission coefficient $C_{adm,1}$. Table 2 shows the mass oscillation and emptying column velocity of Emptying Columns No. 1 and 2.

Table 2. Fundamental equations of the mathematical model of an irregular pipe.

Mass Oscillation No. 1	$\frac{du_{e,1}}{dt} = \frac{p_a - p_{atm}}{\rho_w L_{e,1}} + g\frac{\Delta z_{e,1}}{L_{e,1}} - f_1\frac{u_{e,1}\lvert u_{e,1}\rvert}{2\phi} - \frac{R_v g A_1{}^2 u_{e,1}\lvert u_{e,1}\rvert}{L_{e,1}}$
Emptying Column No. 1	$\frac{dL_{e,1}}{dt} = -u_{e,1}(L_{e,1,0} - \int_0^t u_{e,1}\,dt)$
Mass Oscillation No. 2	$\frac{du_{e,2}}{dt} = \frac{p_a - p_{atm}}{\rho_w L_{e,2}} + g\frac{\Delta z_{e,2}}{L_{e,2}} - f_2\frac{u_{e,2}\lvert u_{e,2}\rvert}{2\phi} - \frac{R_v g A_2{}^2 u_{e,2}\lvert u_{e,2}\rvert}{L_{e,2}}$
Emptying Column No. 2	$\frac{dL_{e,2}}{dt} = -u_{e,2}(L_{e,2,0} - \int_0^t u_{e,2}\,dt)$

In Table 2, u_e = water column velocity, p_a = air pocket pressure, p_{atm} = initial pressure of the air pocket (atmospheric), L_e = water column length, f = friction factor, Δz_e = height difference, R_v = ball valve resistance coefficient, A = pipe cross section, ϕ = inner pipe diameter and g = gravitational acceleration. The subscripts 1 and 2 refers to branches 1 and 2, respectively. The equations defined in the above table correspond to the formulations associated with the water phase. For the air phase simulation, the authors of this mathematical model defined three (3) additional equations. To study the continuity of the air during expansion and admission process through the air valve, the authors of the mathematical model use the following differential equation:

$$\frac{d\rho_{a,1}}{dt} = \frac{\rho_{a,nc} u_{a,nc,1} A_{adm,1}}{A_2(L_2 - L_{e,2}) + A_1(L_1 - L_{e,1})}$$

where ρ_a = air density, $A_{adm,1}$ = air valve cross section and L = branch length. The subscripts 1 = actual conditions and nc = normal conditions. The representation of the evolution of the air pocket during its expansion process is expressed by the following equation:

$$\frac{dp_a}{dt} = -\kappa\frac{p_a(u_{e,1}A_1 + u_{e,2}A_2)}{A_2(L_2 - L_{e,2}) + A_1(L_1 - L_{e,1})} + \frac{p_a\rho_{a,nc}u_{a,nc,1}A_{adm,1}}{A_2(L_2 - L_{e,2}) + A_1(L_1 - L_{e,1})}\frac{\kappa}{\rho_{a,1}}$$

where κ = polytropic coefficient. For the analysis of the air inflow in irregular pipe, the following expression was used:

$$Q_a = C_{adm,1}A_{adm,1}\sqrt{7p_{atm}\rho_{a,nc}\left[\left(\frac{p_a}{p_{atm}}\right)^{1.4286} - \left(\frac{p_a}{p_{atm}}\right)^{1.714}\right]}$$

where Q_a = air inflow and $C_{adm,1}$ = admission coefficient.

The mathematical model of Coronado-Hernández et al. [17] was performed in the Simulink–Matlab software R2021b Update 4 of Mathworks (Natick, MA, USA), where the Ordinary Differential Equation 23s (ODE23s) was applied and supported by a modified Rosenbrock formula with a resolution of second order. In addition, a variable time step was applied, with a maximum value of 0.01 s.

2.2. Two-Dimensional CFD Model

A two-dimensional CFD model was developed by Paternina-Verona et al. [22] for the numerical resolution of compressible multiphase fluids using OpenFOAM software v2012 of CFD Direct (ICL, Saltburn-by-the-Sea, UK) [26]. Different physical equations were used, such as (i) fluid equations (continuity for compressible fluids, momentum and energy) based on Navier–Stokes equations for compressible flows, (ii) transport equations (Partial Volume Fluid Model (PVoF)) [27,28], and (iii) thermodynamic equations for air

phase. Equations (1) and (2) show the formulation of mixing density and viscosity using a phase fraction of water (α_w), and Equation (3) corresponds to the transport equation of PVoF:

$$\rho = \alpha_w \rho_w + (1 - \alpha_w)\rho_a \tag{1}$$

$$\mu = \alpha_w \mu_w + (1 - \alpha_w)\mu_a \tag{2}$$

$$\frac{\partial \alpha_w}{\partial t} + \nabla \cdot (\alpha_w \mathbf{u}) + \nabla \cdot ((1 - \alpha_w)\alpha_w u_r) = 0 \tag{3}$$

where μ = dynamic viscosity, $\mathbf{u}$ = velocity vector, and u_r = velocity source. Fluid equations are fundamental to represent the fluid dynamics during their physical interaction in the geometrical domain, with Equation (4) being the principle of conservation of mass and Equation (5) being the principle of conservation of momentum:

$$\frac{\partial \rho}{\partial t} + \nabla \cdot (\rho \mathbf{u}) = 0 \tag{4}$$

$$\frac{\partial (\rho \mathbf{u})}{\partial t} + \nabla \cdot (\rho \mathbf{u}\mathbf{u}) = -\nabla p + \nabla \cdot (\mu \nabla \mathbf{u}) + \rho \mathbf{g} - F_s \tag{5}$$

where p = static pressure and F_s = surface tension. To guarantee the thermodynamic and mechanical interaction of the fluids, the energy conservation equation (Equation (6)) and the equation of state of air (Equation (7)) were added. On the other hand, the density of water was simulated as a constant value, because changes in density with respect to physical changes in mechanical and thermodynamic origin can be considered negligible in this fluid:

$$\frac{\partial (\rho e)}{\partial t} + \nabla \cdot (\rho e \mathbf{u}) = \nabla \cdot \mathbf{q} + p(\nabla \cdot \mathbf{u}) + S_T \tag{6}$$

$$\rho_a = \frac{p_a}{R T_a} \tag{7}$$

where e = specific energy, $\mathbf{q}$ = heat flux and S_T = energy source term. Turbulence equations were based on the SST k–ω model of Menter [29,30] complemented with wall functions [31]. The turbulence equations of SST k–ω were used based on the advantages offered by these equations in the simulation of turbulent effects, especially those of admitted air, i.e., (i) adequacy in aerodynamic flows, (ii) presence of adverse pressure and velocity gradient, and (iii) adequate representation of the boundary layer (logarithmic region and viscous sub-layer), being an analysis with low sensitivity to dimensionless distance (y^+). Equations (8) and (9) show mathematical formulations of generation and dissipation of turbulence, respectively (all terms are mentioned in the notation section for the purpose of brevity):

$$\frac{D(\rho k)}{Dt} = S_k - \beta^* \rho k \omega + \nabla \cdot (\rho D_k \nabla k) - \frac{2}{3}\rho k (\nabla \cdot \mathbf{u}) + \rho G \tag{8}$$

$$\frac{D(\rho \omega)}{Dt} = \nabla \cdot (\rho D_\omega \nabla \omega) + \frac{\rho \gamma G}{\nu_t} - \frac{2}{3}\rho \gamma \omega (\nabla \cdot \mathbf{u}) - \rho \beta \omega^2 + S_\omega + \rho (1 - F_1) C D_{k\omega} \tag{9}$$

The numerical approximation was carried out by means of the Pressure-Implicit with Splitting of Operators (PISO) algorithm, using numerical schemes of first order for the solution of divergence and temporal terms of equations, as well as second order schemes for the solution of the Laplacian and gradient terms.

The CFD numerical model presented three boundaries: (1) inlet and (2) outlet, which were exposed to atmospheric conditions, with the first one being the air admission area and the second one being the water drainage area, and, additionally, (3) the walls to guarantee flow restriction within the geometrical domain. The boundaries of the CFD model were calculated by applying the mathematical formulations described in Table 3.

Table 3. Mathematical equations for boundaries of the CFD model [26].

Variable	Inlet	Outlet	Walls
p (Pa)	$p_{inlet} = p_{atm} - 0.5\rho u^2$	$p_{outlet} = p_{atm} - 0.5\rho u^2 - \rho g \Delta h$	$p_{walls} = p_{atm}$
u (m/s)	$u_{inlet} = u_{inlet,0} - \frac{p_{inlet} - p_{inlet,0}}{\rho u_{inlet,0}}$	$u_{outlet} = u_{outlet,0} - \frac{p_{outlet} - p_{outlet,0}}{\rho u_{outlet,0}}$	$u_{walls} = 0$

In Table 3, p_{inlet} = calculated pressure at the inlet boundary, p_{outlet} = calculated pressure at the outlet boundary and p_{walls} = calculated pressure at walls. On the other hand, u_{inlet}, u_{outlet} and u_{walls} correspond to calculated velocities at the inlet, outlet and walls boundaries, respectively, and the subscript zero (0) corresponds to the calculated values of the previous iteration. The term Δh refers to the difference in height of the fluid contained on the outlet boundary.

A structured mesh was used to simulate the transient flows using different mesh blocks, with refinements in the area of the pipe walls with an aspect ratio of 1:3. The mesh sensitivity analysis was performed based on a 2D CFD model performed in the research of Paternina-Verona et al. [23], where the authors developed tests with different meshes between 9218 and 65,855 cells, with a mesh of 20,289 cells offering a good numerical fit. In this sense, in this research, a total of 29,909 cells were defined in the computational domain. Figure 2 shows the computational domain of the 2D CFD model.

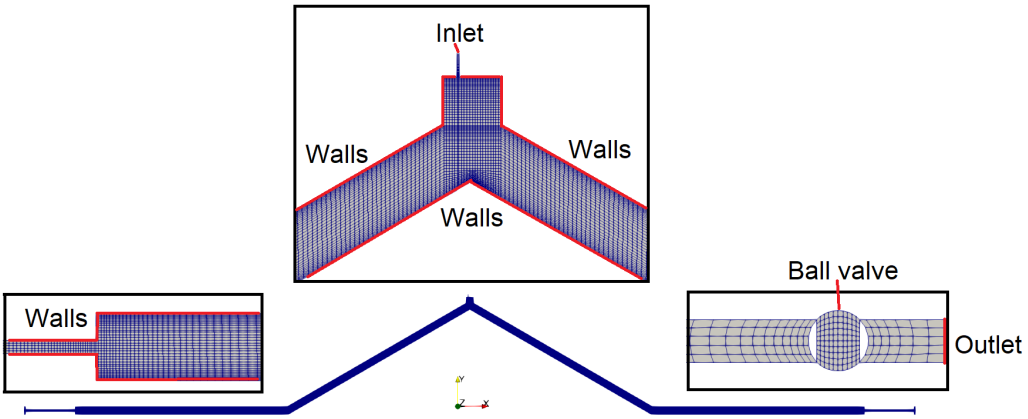

Figure 2. CFD computational domain of an irregular pipeline.

For the computational execution, a maximum Courant number of 0.5 was used, with an initial and minimum time step $\Delta t_{min} = 10^{-4}$ s, which was automatically adjusted with run time up to a maximum time step $\Delta t_{max} = 1.0$ s. This took into account the physical evolution of the interaction between water and air in the computational domain, which improved the computational efficiency and numerical stability of the simulation. As a convergence criterion, the evolution of the residuals of the pressure variable p was analysed. In general terms, the initial pressure residual decreased to a value on the scale of 10^{-4} Pa, and final residuals tended to values of pressure on the scale of 10^{-7}. The numerical solution of the pressure reached convergence in 1 to 2 iterations, which indicated a quick convergence. Finally, 2D CFD models were executed in an AMD Ryzen 5 3500U processor, (Advanced Micro Devices, Inc., Santa Clara, CA, USA), with a frequency of 2.3 GHz, 4 cores, 8 threads, and a memory of 8 GB.

2.3. 2D CFD Model vs. Mathematical Model

The CFD model represented a two-dimensional analysis of the emptying process of an irregular pipeline with air valves, for which it was numerically validated with experimental measurements. Additionally, the calibration of a geometric aspect ratio used for the simulation of the air admission orifice was performed, and the influence of the air valve sizing on the subatmospheric pressures, emptying velocity and water column

length was analysed. Numerical information of pressure and velocity was extracted with a point located in the upper end of the geometric domain of the 2D CFD model to evaluate pressure oscillations (similar to the location of the pressure transducer) and a point located in the right horizontal branch of the pipeline to evaluate water drainage velocity (similar to the location of the UDV device). This numerical information presented an outstanding numerical error margin, according to the contribution of Paternina-Verona et al. [22], where numerical errors ranged from 0.07% to 3.7%, which are acceptable values from the numerical point of view, as evidenced in the contributions made by Besharat et al. [20]. Mathematical models and 2D CFD models have in common the capability of obtaining good numerical results, which is evidenced by the pressure patterns in Figure 3 and in the drainage velocity patterns in Figure 4, corresponding to the simulation in tests presented in Table 1.

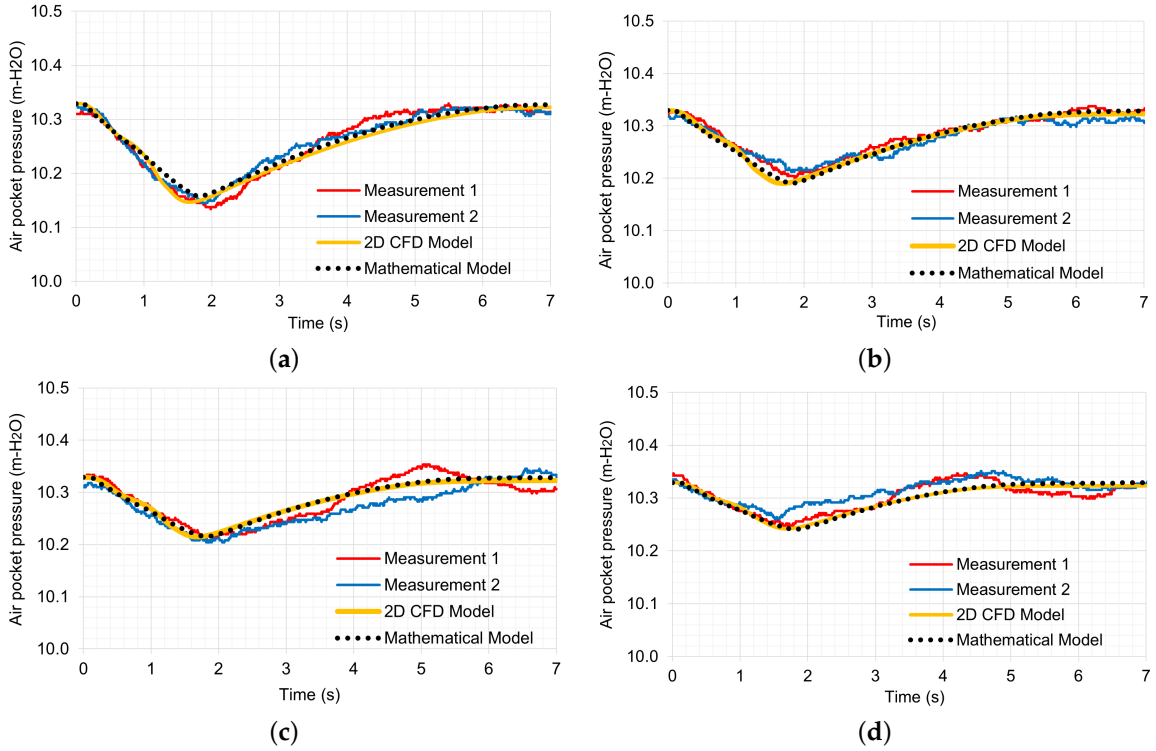

Figure 3. Comparison of pressure patterns of (**a**) Test 1-1, (**b**) Test 1-2, (**c**) Test 1-3 and (**d**) Test 1-4 (Experimental model, 2D CFD model and mathematical model).

With the information from the pressure patterns of the experimental model and the numerical models (mathematical and CFD models), it was possible to identify the minimum pressure value identified in the hydraulic system, which allowed us to observe the influence of the size of the trapped air pockets in the generation of negative pressures that can threaten the hydraulic system. In this case, Tests 1-1, 1-2, 1-3 and 1-4 reach minimum pressure values of 10.15, 10.19, 10.21 and 10.24 m of H_2O (m-H_2O), respectively.

Additionally, it was possible to validate the use of the turbulence equations in the CFD model with the data on the water drainage velocity, taking into account the peak velocity values presented in all tests. Maximum values of the Reynolds number were identified in this hydraulic system using the Reynolds formula (Equation (10)):

$$R_e = \frac{u_{max}\phi}{\nu_w} \tag{10}$$

where ϕ = 0.0514 m and $\nu_w = 1 \times 10^{-6}$ m^2/s at T = 20 °C. Table 4 shows the Reynolds number results for the different tests of the irregular pipe, in which maximum values

between 13,415 and 21,198 were present, which are part of the turbulent flow regime, validating the use of a turbulence model for the CFD modelling.

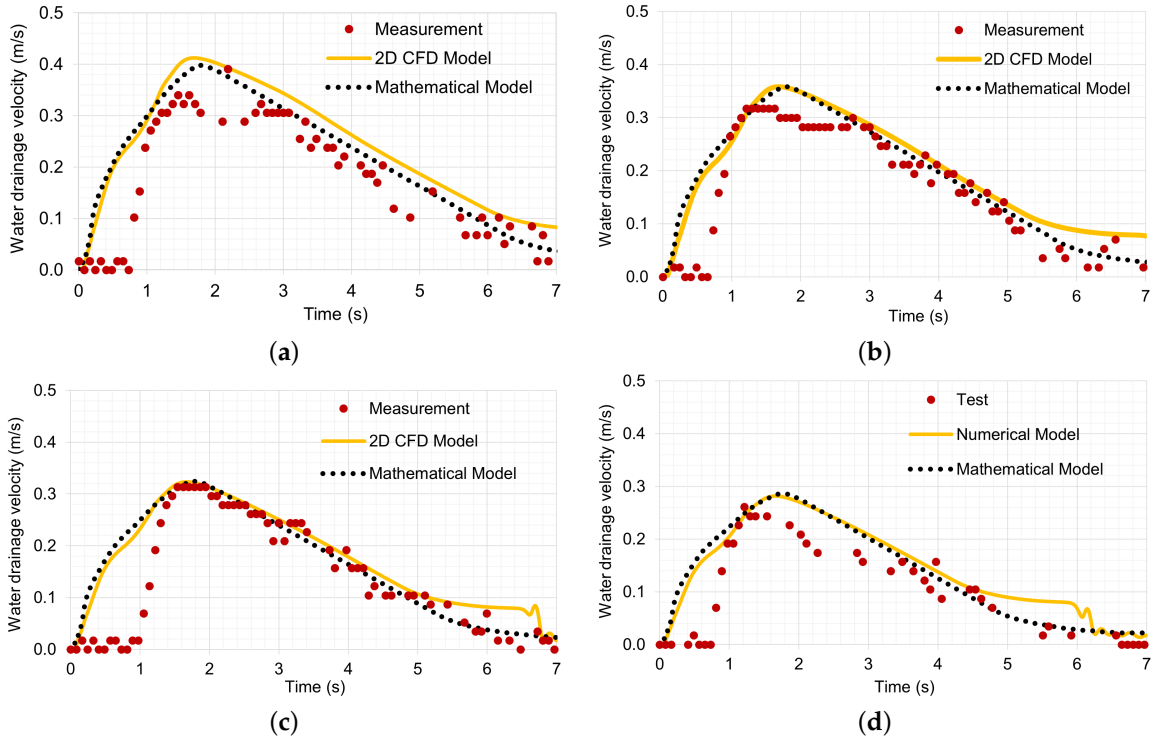

Figure 4. Comparison of velocity patterns of (**a**) Test 1-1, (**b**) Test 1-2, (**c**) Test 1-3 and (**d**) Test 1-4 (Experimental model, 2D CFD model and mathematical model).

Table 4. Maximum water drainage velocities and Reynolds number obtained in the emptying tests of an irregular pipe (u_{max} in m/s).

Test	u_{max} (Exp.)	R_e (Exp.)	u_{max} (Math.)	R_e (Math.)	u_{max} (CFD)	R_e (CFD)
1-1	0.391	20,097	0.398	20,467	0.412	21,198
1-2	0.317	16,294	0.358	18,395	0.358	18,410
1-3	0.313	16,088	0.325	16,681	0.323	16,622
1-4	0.261	13,415	0.286	14,705	0.282	14,486

On the other hand, the 2D CFD model shows information concerning air–water interface deformation, such as the air–water interface location, which can be obtained at different time instants, as opposed to the mathematical model. This component is corroborated and validated with video data from experimental tests. Figure 5 shows the air–water interface location of the 2D CFD model of Test 1-1, where a good agreement is shown between the 2D CFD model contours and the screenshots of the video data at different time instants. Concerning the phase fraction of the 2D CFD model (Figure 5), the separation between the two fluids presented an adequate stratification between the trapped air pocket and the water phase, since there was no collapse of this interface.

Different authors in the literature developed mathematical models to study the effect of air admission orifices in different emptying processes to predict the evolution of subatmospheric pressures as a function of the sizing of these protection devices. In addition to predicting the evolution of air pocket pressure patterns under these scenarios, CFD modelling allows us to visualise the dynamic behaviour of the admitted air and its aerodynamic ratio with the entrapped air pocket that expands during drainage events. Figure 6 shows the behaviour of the air pocket and the air-flow admitted by the air valve through streamlines, corresponding to Test 1-1.

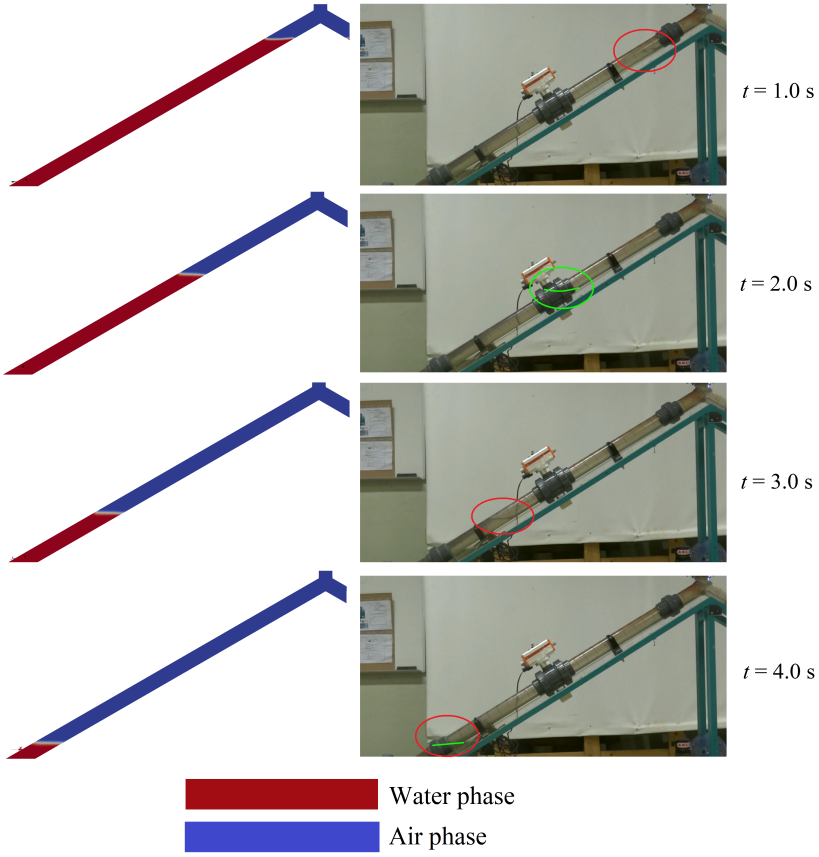

Figure 5. Air–water interface location in 2D CFD model and experimental test (Test 1-1).

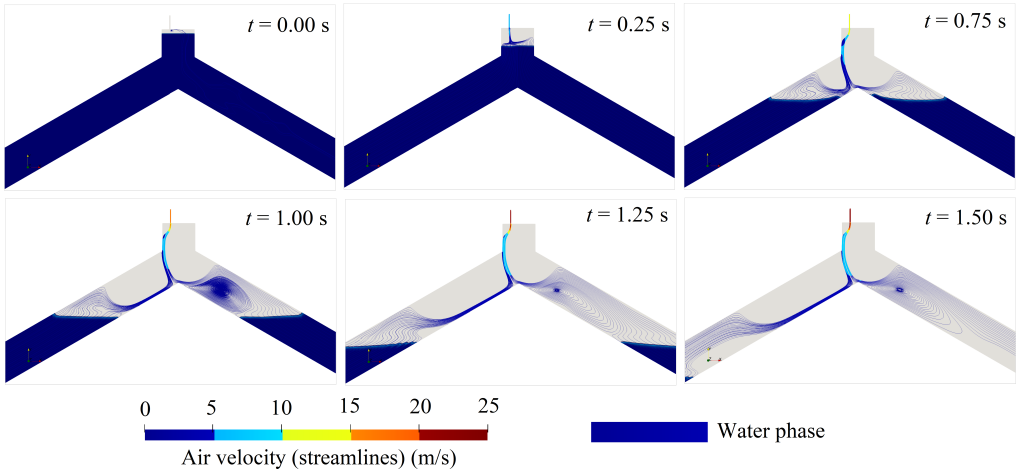

Figure 6. Evolution of the air inflow during the emptying process of the irregular pipeline.

Initially, the pipe is filled with water (there is a small air pocket in the upper zone of the hydraulic system). During the emptying process, air is admitted through the air valve. Subsequently, the air-flow is damped by its impact with the air–water interface at t = 0.25 s. From t = 0.75 s, the air-flow is dispersed towards the pipe branches as a consequence of the impact with the lower vertex of the branch junction. On the right branch of the hydraulic system, an air vorticity phenomenon occurs near the air–water interface from t = 1.0 s. On the other hand, in the left branch, the air-flow is displaced over the lower zone of the pipe cross-section and then damped at the air–water interface. The air-flow velocity inside the pipe tends to decrease as it approaches the air–water interface. At t = 1.25 s, the air-flow velocity admitted in the air valve zone tends to values higher than 20 m/s. Inside the vertex

of the hydraulic system, the air-flow velocity attains values between 5 and 10 m/s, and in the branches of the pipeline, the value of the air-flow velocity decreases to values less than 5 m/s. In this sense, aerodynamic flow in emptying processes of pipelines with air valves represents a significant contribution to verify the design of air valves and their influence on the durability of the hydraulic system, being a physical phenomenon that cannot be identified by mathematical models.

In general, 2D CFD models show velocity, pressure and temperature contours as additional information to the visual information of air–water interface. The 2D CFD model is a more robust model compared to the mathematical model; therefore, it requires more computational time, on the order of minutes up to hours, depending on the conditions of the processor performing such simulations. It is important that the user uses a multi-core processor to facilitate parallel processing. This procedure is one of the determining factors to reduce computational time. Figure 7 shows the execution times for the 1.0 s virtual reality simulation corresponding to the CFD model of Test 1-1, performing simulations with different numbers of cores.

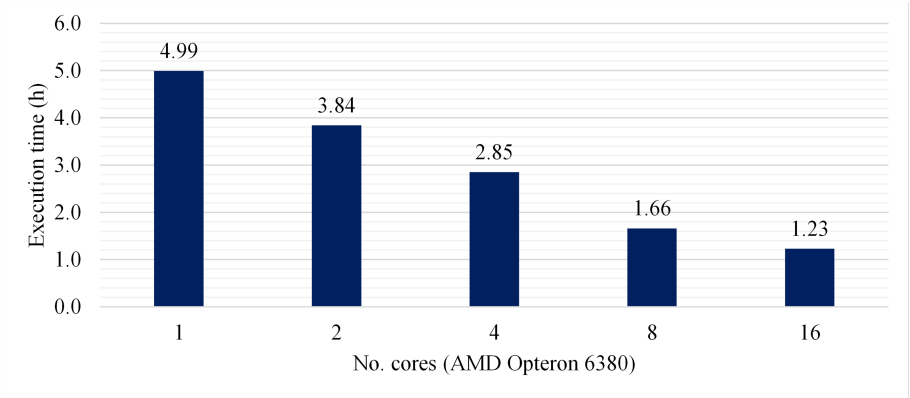

Figure 7. Execution time for simulation of 1.0 s in a 2D CFD model.

Parallel processing of a CFD model simulation in the OpenFOAM software , and on a medium- or high-performance computer, allows the user to reduce significant computational time. Figure 7 shows that, for simulations in an AMD(R) Opteron(TM) 6380 processor (Advanced Micro Devices, Inc., Santa Clara, CA, USA), the 1.0 s virtual reality simulation of Case 1 is reduced from 5 to 1.23 h, when splitting the simulation process from 1 to 16 cores. A multi-core processor can be a tool that guarantees a reduction in computational time with better CPU utilisation. Although the CFD model requires more computational time, it is adequate to perform parallel simulations through multi-core processors with high computational performance, a condition that applies to both 2D and 3D CFD modelling.

3. Numerical Modelling in Single Pipelines

In this scenario, an experimental setup of a single pipe with a trapped air pocket at one upper end upstream and an internal diameter of 42 mm was carried out. The experimental setup corresponds to a main linear section with a length of 4160 mm, and a complementary section of 200 mm long, interconnected with the main linear section through a 90° elbow. Different emptying processes were tested using different values of L_{iap}, ball valve opening degrees (τ), and ball valve opening times (t_m). From this experimental setup, the emptying processes associated with two scenarios were explored: (i) Case 1—without air admission orifice and (ii) Case 2—with air admission orifice. As a measurement parameter, a pressure transducer located at 0.105 m from the upstream end of the pipeline was used to measure the pressure oscillation of trapped air from t = 0 with a frequency of 7000 Hz. Figure 8 shows the installation and description of the elements used in the experimental setup, followed by Table 5, which shows the results four (4) tests, where Tests C1-1 and C1-2 correspond to Case 1, and Tests C2-1 and C2-2 correspond to Case 2.

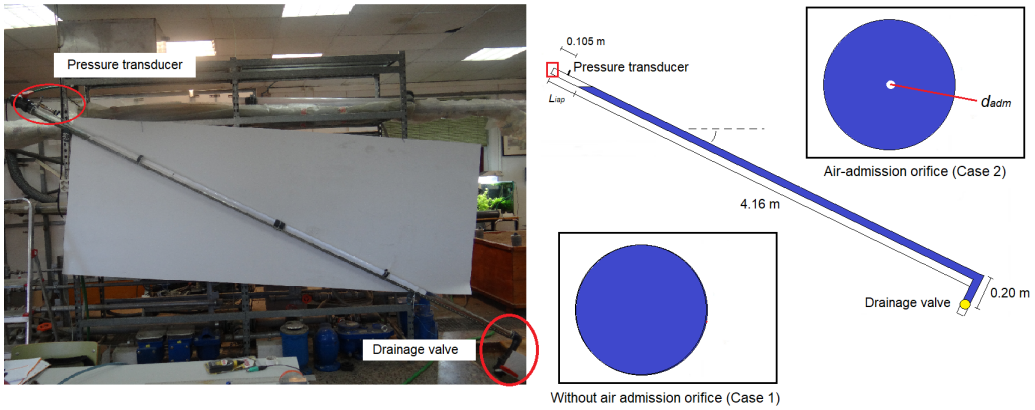

Figure 8. A single pipeline with Case 1 (without air valves), and Case 2 (with air valves).

Table 5. Initial conditions of the single pipe experimental tests—Cases 1 and 2.

Parameter	Test C1-1	Test C1-2	Test C2-1	Test C2-2
L_{iap} (m)	0.45	0.205	0.205	0.45
t_m (s)	0.50	0.30	0.50	0.40
τ (%)	12.0	6.0	24.5	13.4
d_{adm} (mm)	–	–	3.0	3.0

3.1. Mathematical Model of Single Pipelines (Cases 1 and 2)

The mathematical model of Fuertes-Miquel et al. [18] was used as reference, which represents a model of single pipe that contains an air pocket and a water column. This model considers the same assumptions mentioned in the mathematical model of Coronado-Hernández et al. [17] concerning the mass oscillation and emptying column equations, as shown in Table 6.

Table 6. Fundamental equations of the mathematical model.

Mass oscillation	$\frac{du_e}{dt} = \frac{p_a - p_{atm}}{\rho_w L_e} + g\frac{\Delta z_e}{L_e} - f\frac{u_e\lvert u_e\rvert}{2\phi} - \frac{R_v g A^2 u_e\lvert u_e\rvert}{L_e}$
Water column length	$\frac{dL_e}{dt} = -u_e(L_{e,0} - \int_0^t u_e\, dt)$

To analyse the physical behaviour of trapped air in Case 1, an equation was added as a function of air pocket length (L_{ap}) and polytropic coefficient (κ), as shown in Equation (11):

$$p_a {L_{ap}}^{\kappa} = p_{atm} {L_{iap}}^{\kappa} \tag{11}$$

On the other hand, for the simulation of trapped air considering an air admission orifice in the single pipe (Case 2), Fuertes-Miquel et al. [18] defined three (3) equations: (i) a mass conservation equation (Equation (12)), (ii) a polytropic equation considering mass oscillations over time (Equation (13)) and (iii) a mass flow equation for the air inlet orifice simulation, as shown in Equation (14):

$$\frac{dm_a}{dt} = \frac{d\rho_a}{dt} V_a + \frac{dV_a}{dt}\rho_a \tag{12}$$

$$\frac{dp_a}{dt} = -\kappa\frac{p_a}{V_a}\frac{dV_a}{dt} + \frac{p_a}{V_a}\frac{\kappa}{\rho_a}\frac{dm_a}{dt} \tag{13}$$

$$Q_a = C_{d,adm} A_{adm} \sqrt{7 p_{atm} \rho_a \left[\left(\frac{p_a}{p_{atm}}\right)^{1.4286} - \left(\frac{p_a}{p_{atm}}\right)^{1.714} \right]} \tag{14}$$

This mathematical model by Fuertes-Miquel et al. [18] used a similar computational setup to the mathematical model presented by Coronado-Hernández et al. [17] described in Section 2.1.

3.2. Three-Dimensional CFD Model

As with the two-dimensional CFD model described in Section 2 of this research, Paternina-Verona et al. [8,24] ensured the numerical solution of the fluid, PVoF, transport and thermodynamic equations using OpenFOAM software v2012 of CFD Direct (ICL, UK) for application on a three-dimensional computational domain. To simulate the turbulence, SST k–ω model was used, based on the advantages of this model mentioned in Section 2.2, taking into account that these equations have been used by other authors to analyse two-phase transient flows in three-dimensional CFD models [25,32].

First and second order numerical schemes were defined in the different terms of the governing equations, and the PISO algorithm was used. Cases 1 and 2 correspond to a similar experimental setup, so the difference between models is highlighted by the presence of the orifice. In Case 1, the CFD model has four boundaries: (i) outlet, (ii) walls, (iii) moving walls and (iv) Valve Sliding Interface (VSI); in Case 2, the boundary conditions of Case 1 were used, adding a boundary corresponding to Inlet (air admission orifice). Equations of boundary conditions were similar to those presented in Table 3, where the VSI boundary in contact with the pipes allowed flow circulation to aid water drainage and acted as a wall when the ball valve connections were not in contact with the pipeline.

The CFD model was performed using a structured mesh in all geometric domains: in Case 1, using a square cross-section within the circular cross-section, and for Case 2, using a detailed orifice with small cells, with a cell had a dimension of 3×10^4 m in width. These details are shown in Figure 9.

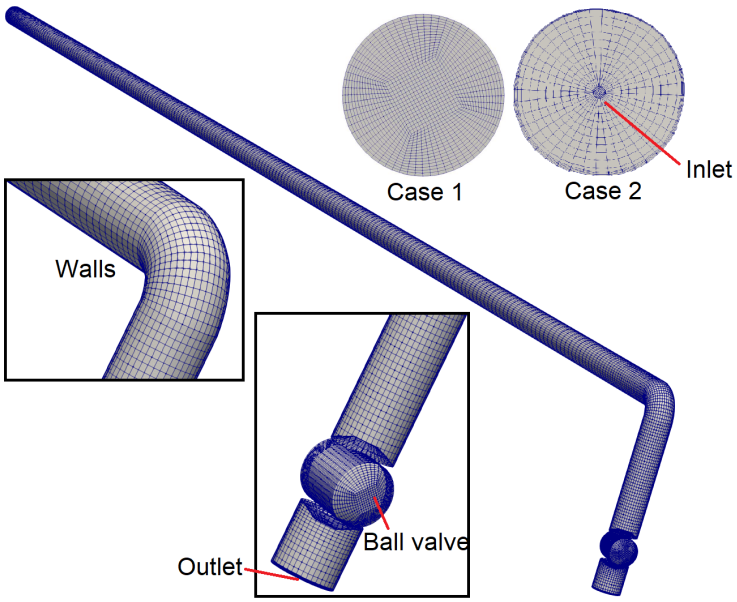

Figure 9. Geometric domain of 3D CFD model applied for Cases 1 and 2.

A sensitivity analysis of the mesh was performed to verify the independence of the numerical results from the mesh resolution. To that end, Paternina-Verona et al. [8] performed an independence analysis of this CFD geometry through the analysis of the numerical evolution of the pressure patterns using different meshes, ranging from 43,500 to 1,220,000, cells with different meshing properties (aspect ratio, asymmetry, orthogonality and computational times), where the numerical results with the different meshes presented a good agreement with the reference measurement used. Finally, in this research, a mesh of 507,375 cells was used for Case 1 and a mesh of 173,500 cells in Case 2 [24].

In addition, a maximum Courant number of 0.5 was used, with an adjustable time step between 10^{-4} s and 1.0 s, similar to the 2D CFD model performed in Section 2.2. To verify the convergence of the numerical solution of the CFD model, the decrease in the residuals of the pressure variable was verified, in which the residuals generated in the 3D CFD models of Case 1 tended on average to values that oscillated on the scale of 10^{-4} Pa, in which the numerical solution of this variable converged after a maximum of 8 iterations. On the other hand, the residuals of the 3D CFD models of Case 2, at a general level, tended to values that oscillated on the scale of 10^{-5} Pa, reaching convergence after a maximum of 2 iterations. These simulation were executed in an AMD(R) Opteron(TM) 6380 processor, with a frequency of 2.75 GHz, 16 cores, 32 threads and physical memory of 96 GB.

3.3. 3D CFD Model vs. Mathematical Model

In order to compare the 3D CFD model with the information provided by the mathematical model of Fuertes-Miquel et al. [18], a single pipe without air admission orifice was used as a case study. Tests C1-1 and C1-2 were simulated for 3 s, and Tests C2-1 and C2-2 were simulated until the pipes were drained. Case 1 tests were run up to an instant t = 3 s since, experimentally, the water column could not be drained due to subatmospheric pressures. In addition, numerical information of pressure oscillations of 3D CFD models were extracted with an internal point located at 0.105 m from the upper end of the pipeline (similar to the location of pressure transducer).

The 3D CFD model was performed, which showed a variety of relevant information that these models offer under a three-dimensional domain, providing an approximation to real conditions. In this model, different hydraulic and thermodynamic phenomena, such as (i) deformation of the air–water interface, (ii) backflow air (DAPs), (iii) transient flows, (iv) velocity distribution curves in different sectors of the pipe due to the influence of backflow air and (v) velocity and temperature distribution in cross-sections were seen in detail (see these in more detail in the contribution of Paternina-Verona et al. [8]).

The pressure oscillations of the mathematical model and the 3D CFD model were compared to show the similarity between the results, as shown in Figure 10.

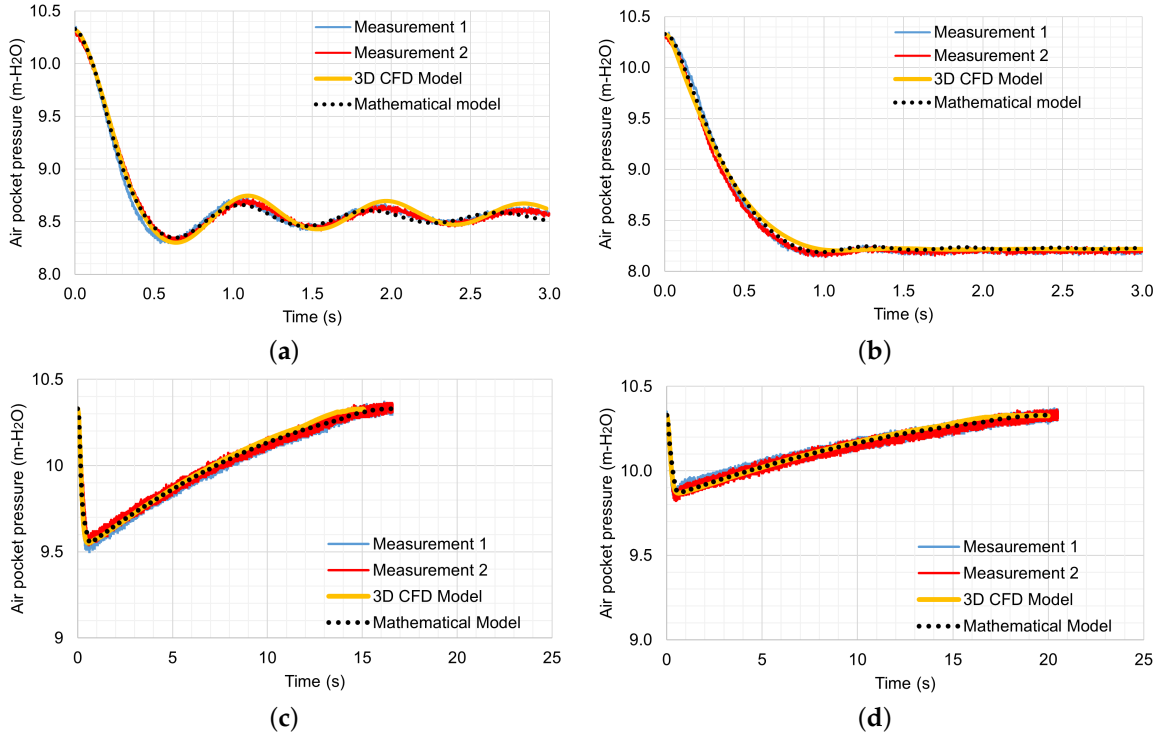

Figure 10. Comparison of pressure patterns of (**a**) Test C1-1, (**b**) Test C1-2, (**c**) Test C2-1 and (**d**) Test C2-2 (3D CFD model vs. mathematical model).

In Test C1-1 (Figure 10a), a critical subatmospheric pressure occurred at t = 0.64 s, where the minimum value reached by the mathematical model was 8.34 m-H_2O, and the value of minimum pressure in the CFD model reached a maximum value of 8.29 m-H_2O. Subsequently, it was identified that the CFD model predicted the behaviour of the pressure oscillations recorded by the mathematical model which occurred after the minimum pressure value. It was possible to identify that the pressure oscillations in the CFD model presented a delay in their peaks and valleys with respect to the oscillations detected by the mathematical model, an effect that is mainly influenced by the backflow air phenomenon. On the other hand, in Test C1-2 (Figure 10b), with a lower valve opening degree than Test C1-1, a good agreement with the pressure oscillations of the mathematical model was presented, reaching a minimum pressure of 8.20 m-H_2O.

Tests C2-1 and C2-2 (scenarios with air admission orifices) were also compared, where CFD model results were similar to pressure patterns of the mathematical model. In Test C2-1 (Figure 10c), the emptying process resulted in an expansion of the trapped air, reaching a minimum pressure of 9.55 m-H_2O at t = 0.58 s and then gradually rising until it reached atmospheric pressure again at t = 16 s, which coincided with the instant of time at which the pipe had been completely drained. On the other hand, Test C2-2 (Figure 10d) showed a decrease in trapped air pressure, down to a minimum value of 9.87 m-H_2O at t = 0.60 s, then returning to atmospheric pressure after t = 18 s.

In addition to pressure patterns, the water flow patterns obtained from the 3D CFD model were compared with the results of the mathematical model, using all tests of this scenario. Figure 11a shows the flow patterns of Test C1-1 of the CFD model, compared with the results of the mathematical model associated with the test in reference. Transient flow with higher amplitudes compared to the mathematical model were observed, except for the first flow peak, for which there was a maximum value of 0.29 L/s in the mathematical model, and a value of 0.22 L/s in the 3D CFD model. There were maximum peaks in the flow patterns of the mathematical model and the 3D CFD model of 0.08 and 0.11 L/s, respectively, in Test C1-2 (Figure 11b). In this case, the peak flow of the three-dimensional CFD model was greater than the peak flow of the mathematical model. In Test C2-1 (Figure 11c), water flow patterns of the mathematical and CFD models showed good agreement in their physical behaviour, whereas the mathematical model predicted a peak discharge flow of 0.636 L/s, while the peak discharge flow predicted by the 3D CFD model was 0.632 L/s. Finally, in Test C2-2 (Figure 11d), the numerical pattern of the CFD model adequately predicted the trend of the volumetric flow rate of the mathematical model, presenting a good agreement in the physical behaviour. On the one hand, the mathematical model of Test C2-2 reached a maximum flow rate of 0.49 at t = 0.465 s, whereas the 3D CFD model predicted two maximum peaks flows with values of 0.50 L/s at t = 0.27 s and 0.516 L/s at t = 1.15 s.

In addition, the utilisation of the turbulence model was validated as a function of the maximum Reynolds number presented in the different tests, given through the information of the maximum flow rate and the hydraulic section for diameter ϕ = 0.042 m. Table 7 shows the general distribution of the maximum Reynolds numbers predicted in each numerical model, where the range presented was from 2.667 to 19.183, so the hydraulic scenarios were in the turbulence and transition region, which are suitable indicators to validate the use of the SST k–ω turbulence model.

Table 7. Maximum water drainage velocities and Reynolds numbers obtained in emptying tests of a single pipe ($Q_{w,max}$ in units of L/s).

Test	$Q_{w,max}$ (Math.)	R_e (Math.)	$Q_{w,max}$ (CFD)	R_e (CFD)
C1-1	0.286	8682	0.223	6760
C1-2	0.088	2677	0.110	3335
C2-1	0.636	19,285	0.632	19,183
C2-2	0.490	14,871	0.516	15,660

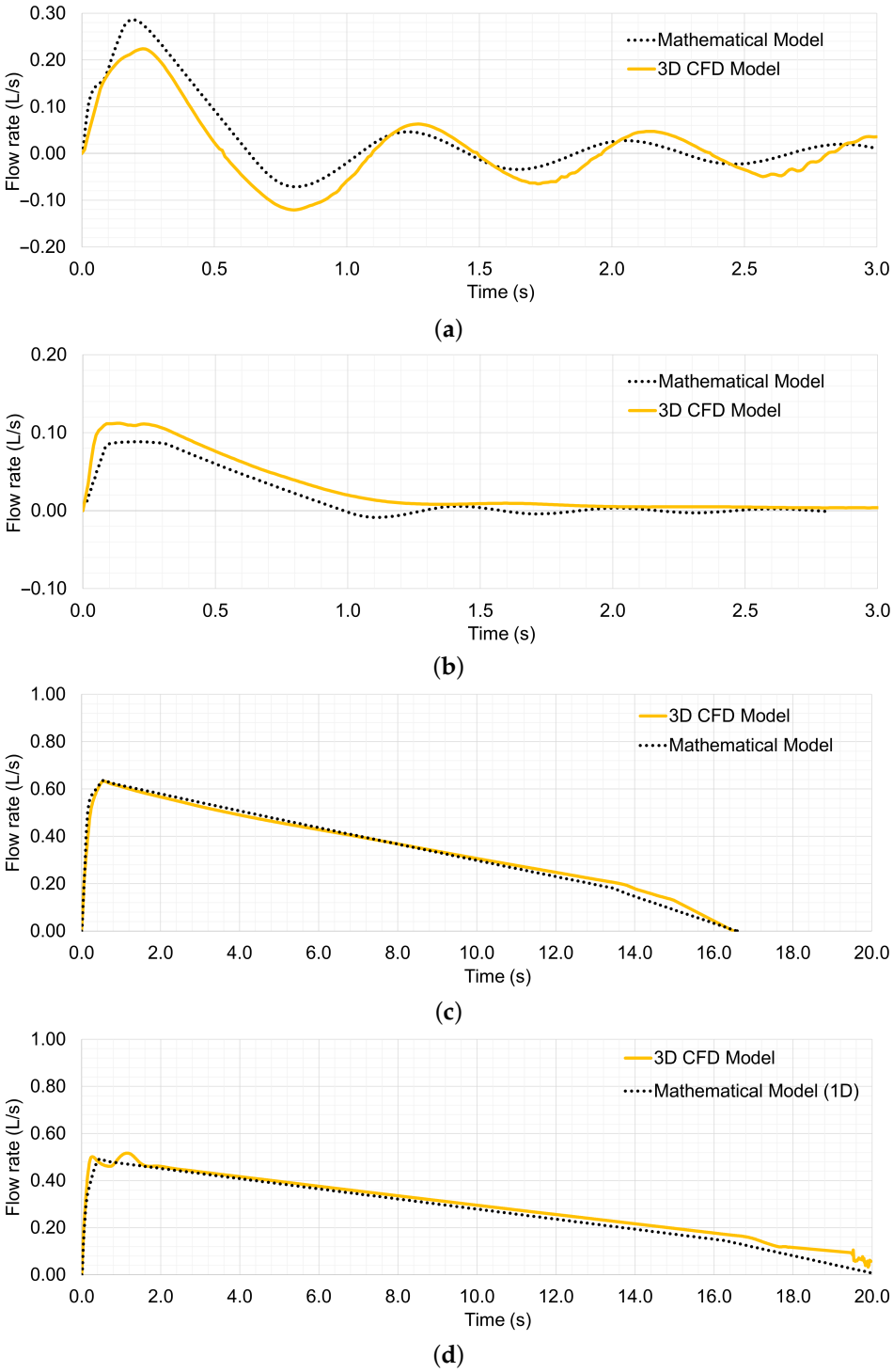

Figure 11. Comparison between water flow patterns during emptying processes of a single pipe. (**a**) Test C1-1, (**b**) Test C1-2, (**c**) Test C2-1 and (**d**) Test C2-2.

The water flow patterns during drainage processes obtained from the 3D CFD models show similar behaviour to the results obtained from the mathematical model; nevertheless, there is a difference in the peak flow values of the two models. It is important to mention the difference between the mathematical model and the 3D CFD model, in terms of the influence on water flow patterns, which is based on the simulation conditions of the ball valve opening percentage. The mathematical model considers the addition of a coefficient of resistance (R_v) equivalent to the head losses generated by the opening percentage of the ball valve. The value of R_v is variable from t = 0 s to the end of the opening manoeuvre, which

depends on the degree of opening at different time instants. On the other hand, the 3D CFD model uses a solid-body motion function to simulate the ball valve through a cylinder with curved surfaces. When the cylindrical mesh contacts the pipes in the 3D CFD model, it allows water to pass between the upstream and downstream sections. Proper simulation of a valve opening manoeuvre has been a challenge in modelling, since it is a manual procedure in practice and susceptible to errors during its representation in hydraulic models. A correct simulation of the ball valve-opening manoeuvre guarantees a higher accuracy of the results and allows an adjustment of the model to real hydraulic conditions.

Differences between oscillations in water flow and pressure patterns in the CFD and mathematical models were also due to the effect of backflow air, which influences the hydraulic conditions of drainage, a phenomenon that was not considered in the physical equations of the mathematical model. This delay in the drainage pressure and flow rate oscillations was significantly evidenced in Test C1-1 (see Figures 12 and 13), which is influenced by the presence of air bubbles entering upstream. It could be observed that the 3D CFD model was able to adequately represent the behaviour of the air pocket, i.e., the movement of the backflow air, forming an appropriate stratification of air pockets, wherein the mixing of these fluids is rarely generated. In contrast, there were no air bubbles in Test C1-2. This is evident in the good agreement between the pressure oscillations and water discharge flow rate of the CFD model with the recorded oscillations of the mathematical model (see Figure 11d).

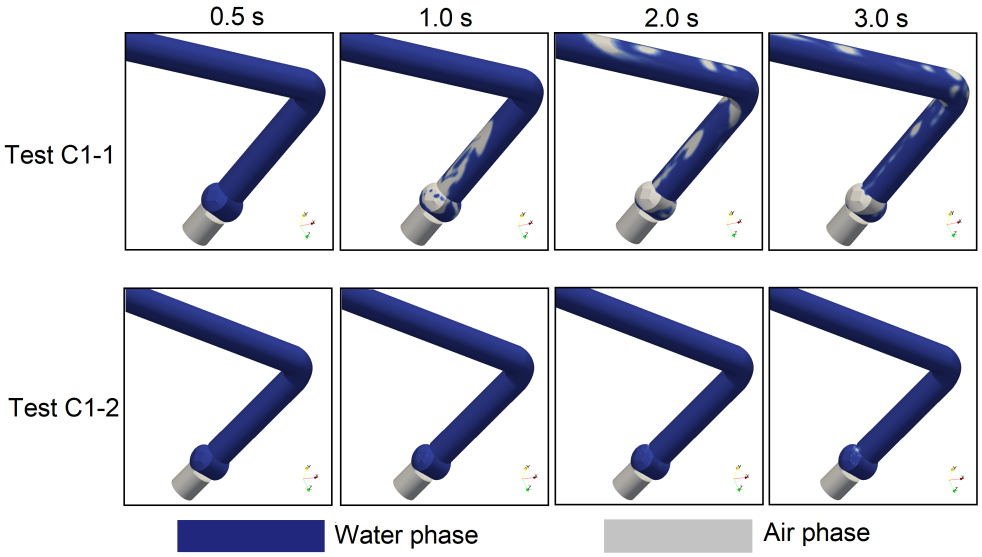

Figure 12. Air intrusion due to backflow air in 3D CFD Model (Tests C1-1 and C1-2).

On the other hand, the thermodynamic behaviour between air and water corresponds to a phenomenon that can be captured by 3D CFD models, which has been rarely studied in the literature. Zhou et al. [33] performed a study of the heat transfer between the air and water phases in a rapid filling process and compared with experimental results through the development of a 3D CFD model, which observed an increase in the temperature of the entrapped air pocket to values of more than 100 °C, which could be observed during the experimental measurements performed. Currently, there are no detailed studies of the thermodynamic behaviour between the air and water phases in pressurised pipe emptying processes. The water phase is characterised by a lower compressibility than the air phase, so its temperature variations are insignificant during transient events. However, the water phase plays an important role in the heat transfer process, as shown in Figure 14, where the temperature gradients that occur from the water phase to the air phase in the emptying processes of Tests C1-1 and C1-2, respectively, are visualised. Additionally, this information is complemented with the air–water interface location during the thermodynamic interaction.

Figure 13. Air intrusion in Test C1-1 (Experimental Model).

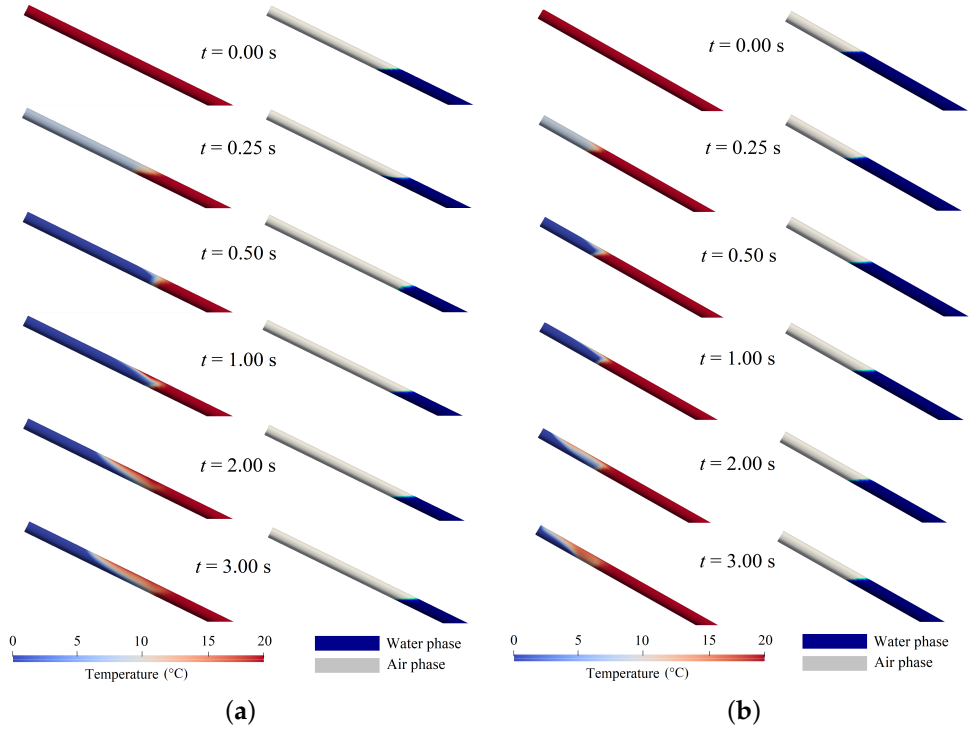

Figure 14. Heat transfer between the water phase and the air phase. (**a**) Test C1-1 and (**b**) Test C1-2.

Figure 15 shows the variation in the temperature patterns in the air pockets of Tests C1-1 and C1-2, where it is observed that the temperature of the entrapped air pockets decreases during the expansion processes, proceeding from 20 °C to minimum values of 1.5 °C and 2.3 °C, respectively, at t = 0.5 and 1.0 s. In Test C1-1, temperature oscillations occur due to the smooth oscillations in the water column velocity, which cause compression of the air pocket, accumulating compression energy that is subsequently transformed into heat energy. In Test C1-2, there is a temperature drop at t = 1.0 s, and, thereafter, the temperature increases progressively, causing the compression and expansion energy to be present in smaller proportions in the air pocket, facilitating its return to ambient temperature by heat transfer between water and air.

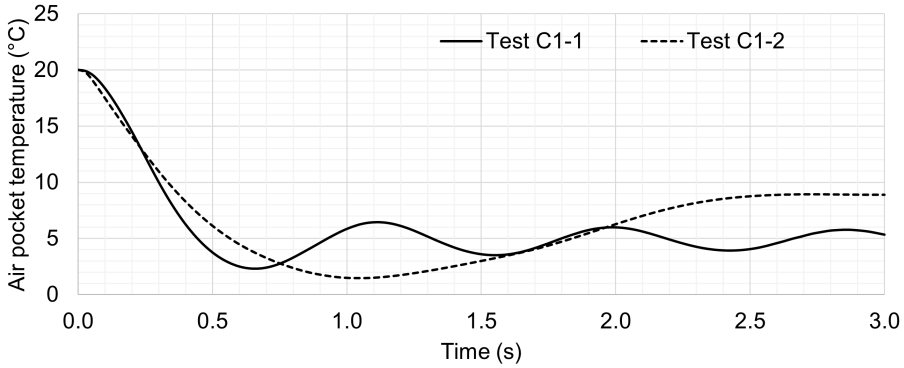

Figure 15. Temperature patterns of the trapped air pocket of CFD model (Tests C1-1 and C1-2).

Comparison of 2D/3D CFD Models

The authors of [23] used an experimental setup similar to the single pipe to represent the scenario associated with Case 2 (emptying process with an air admission orifice), where Test C2-1 was compared with the simulation performed by these authors in their research. An analysis of the physical phenomena in Test C2-1 was performed between the results obtained by the 3D CFD model of Paternina-Verona et al. [24] and the 2D CFD model of Paternina-Verona et al. [23], where the behaviour of the air–water interface and the velocity distribution of the air flow admitted to the hydraulic system through the orifice were compared. Figure 16 showed that the displacement of the air–water interface in the 2D and 3D CFD models was similar at t = 0, 1, 5, and 10 s, and a difference in the location of the air–water interface occurred at the instant t = 15 s, just before total drainage of the water in this test. In this sense, the prediction of the air–water interface can be carried out adequately in both the two- and three-dimensional conditions.

On the other hand, in the 2D and 3D CFD models of Test C2-1, an evaluation of the spatial distribution of the velocity at the upper end of the pipe was carried out, corresponding to the air phase. In order to make an adequate comparison of the velocity gradients between the 2D and 3D CFD models, a cut of the geometry of the 3D CFD model was made on the XY plane to obtain the information of the two-dimensional profile of the pipe axis, as shown in Figure 17.

After cutting on the XY plane, the comparison of the velocity gradients presented in the air admission zone of the single pipe of both CFD models was performed. Figure 18a shows the distribution of velocity produced by the 2D CFD model, where it can be seen that the air admission velocity reached its maximum value at t = 1.0 s and gradually decreased over time, as evidenced at t = 5.0, 10.0 and 15.0 s, a similar trend to the results presented by the 3D CFD model (Figure 18b).

During air admission, three fronts of flow velocity were observed at the upper end of the pipe profile. These fronts reached velocity values between 7 and 10 m/s at the top wall, bottom wall and the central axis of the pipe (see Figure 18a at t = 0.5 and 1.0 s). On the other hand, in the 3D CFD model scenario, a predominant flow velocity front generated by the air admission orifice was observed. This front was attenuated towards the bottom of the upstream end of the pipe, reaching a magnitude greater than 10 m/s. In addition, a small velocity front was generated, which was seen at t = 0.5 and 1.0 s in the upper zone of the upstream end of the pipe (see Figure 18b). In that sense, the velocity contour results of both CFD models presented some discrepancies in terms of the generation of velocity gradients inside the geometrical domain, especially in complex areas such as the air admission orifice. From the above comparison, it was possible to verify some elements that are important to take into account to identify the behaviour of velocity gradients in 2D and 3D CFD models. In particular, 2D CFD models require a geometric aspect ratio to simulate the diameter of the air admission orifice to adjust the mass flow rate conditions, as has been used in previous research [22,34,35], whereas the 3D CFD model allows the generation of an orifice with a diameter equal to the study cases, being an appropriate condition in the evaluation

of diameter changes in pipes. In this regard, the simulation of orifices in 2D CFD models requires a geometric aspect ratio that has been favoured in the representation of emptying processes with admitted air; however, it is an element that must be suitably adjusted during the development of the computational model, depending on the geometric conditions of the pressurised pipes.

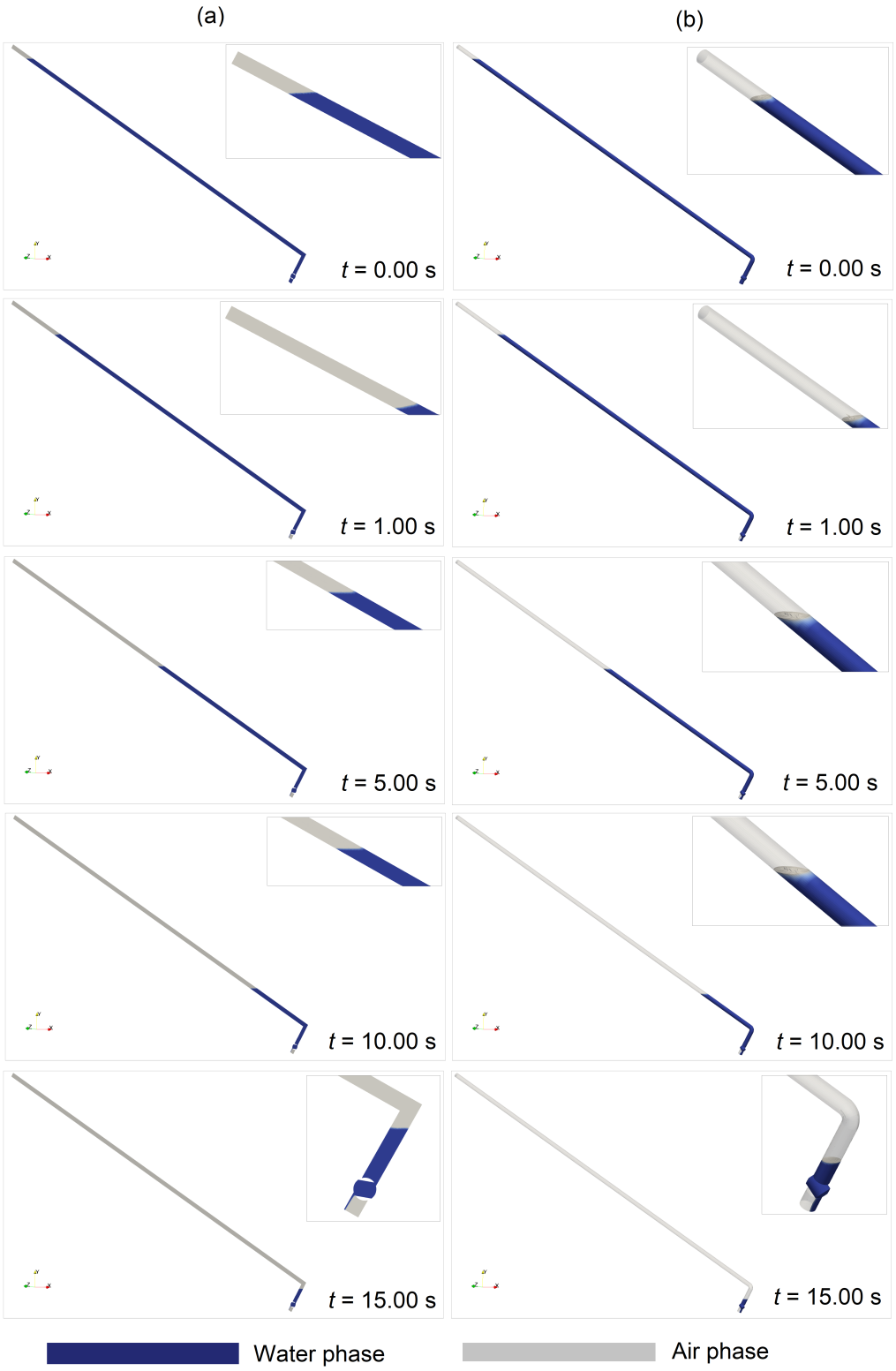

Figure 16. Comparison of air–water interaction of Test C2-1: (**a**) 2D CFD Model [23] and (**b**) 3D CFD Model.

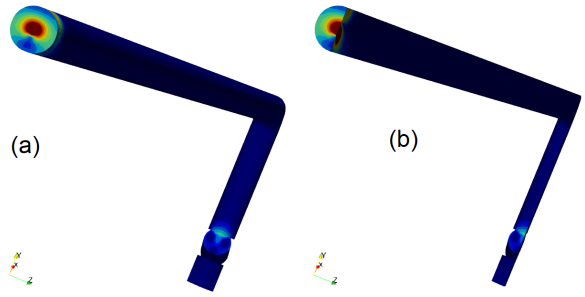

Figure 17. Plane for evaluation of velocity profile in single pipe—Test C2-1: (**a**) Normal 3D CFD model and (**b**) Cut-out of 3D CFD model.

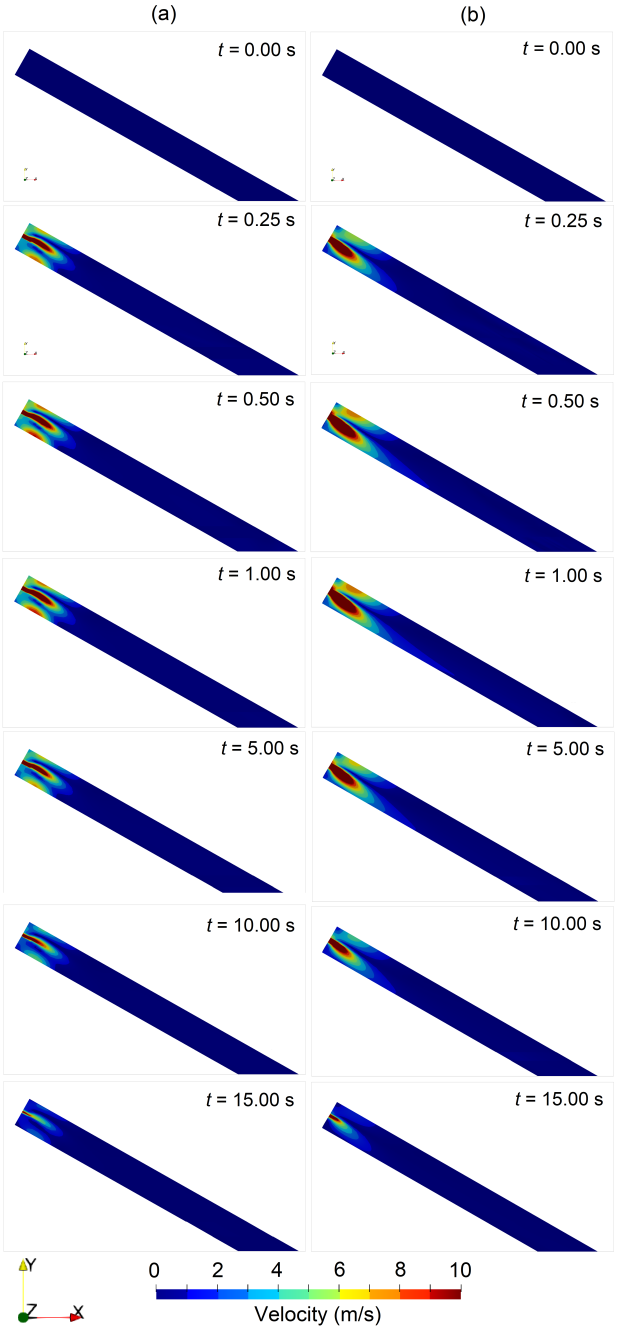

Figure 18. Comparison of velocity contours at upper end of Test C2-1: (**a**) 2D CFD Model [23] and (**b**) 3D CFD Model.

4. Discussion

Numerical models have been useful over the years to facilitate the prediction of hydraulic phenomena in pipelines, serving as an adequate solution to hydraulic engineering problems. The use of these models depends on different user-determined factors, such as (i) physical equations, (ii) level of detail of the information, (iii) use of computational resources, (iv) calibration process and (v) computational simulation time. For example, mathematical models have provided good numerical results for pressure oscillations and discharge water flow in emptying processes, which have also been used in large-scale pipelines through the manipulation or control of the associated physical terms that may be considered in the water and air phases [19,36]. However, these models present restrictions in their use, taking into account that some complex hydraulic and thermodynamic phenomena cannot be predicted in detail or must be assumed in these hydraulic events.

On the other hand, some authors who have developed CFD models to study two-phase transient flows (including emptying operations) highlight the relevant information that these complex models can predict and that the quality of the visual and numerical information is more consistent with what occurs in different experimental cases [8,21,33,37,38]. However, authors who have used CFD models mentioned the complexity of the definition and calibration of these models, as well as the demanding process and computational time required, especially in three-dimensional models, where elements such as (i) the order of solution of numerical schemes, (ii) the algorithm of solution, (iii) turbulence models, (iv) meshing quality, (v) time step and (vi) parallel processing conditions influence the achievement of good numerical and physical results, along with optimisation of computational time.

Detailed knowledge of the advantages and disadvantages of using the different existing numerical models for the study of emptying processes in pressurised pipes could contribute to the appropriate selection of these tools for the solution of hydraulic engineering problems in real pipelines, in addition to verifying and validating possible operational scenarios, including water distribution network design activities. Table 8 defines the advantages and disadvantages of the use of mathematical, 2D CFD and 3D CFD models for the solution of hydraulic engineering problems, focused on the study of emptying processes in pressurised pipes with trapped air, considering the presence or absence of air valves.

Some criteria should be taken into account for the selection of the appropriate numerical model for different studies at the hydraulic engineering level. For example, mathematical models can be applied in cases where hydraulic engineers are only interested in understanding the evolution of certain hydraulic and thermodynamic parameters over time, as well as to identify maximum or minimum values for design and operational efficiency purposes. On the other hand, 2D CFD models can be useful in hydraulic scenarios where it is necessary to identify the motion of the air–water interface and the spatial variation in different variables such as pressure, velocity and temperature in the form of contours on a pipe profile plane (2D plane), in addition to the numerical evolution of these variables at various specific points of the geometric domain over time. Furthermore, 3D CFD models can be adequate in cases where hydraulic engineers require in-detail study of the behaviour of the trapped air volume and its interaction with water installations, in order to obtain a better capture of different hydraulic and thermodynamic phenomena, as well as to observe the evolution of inlet and outlet flows and visualisation of the physical evolution of the variables associated with these fluids using the contours of CFD.

Table 8. Advantages and disadvantages for model development for simulation of emptying processes of pipes with trapped air.

Model	Advantages	Disadvantages
Mathematical model (1D)	Provide accurate and adequate numerical information, where variables such as (i) entrapped air pocket pressure, (ii) water drainage velocity, (iii) water flow rate, (iv) air admission flow rate (in the case of presence of air valves) and (v) temperature can be studied through numerical values that vary as a function of time.	These models do not represent different events that occur during emptying processes, such as (i) backflow air effects, (ii) deformation of the air–water interface and (iii) velocity and temperature gradients.
	These models are easy to implement and require fewer computational resources; their results are obtained in a few seconds.	The water column is considered a rigid uniform column; water velocity is equal at different points in the water column.
	The modelling equations can be manipulated.	
2D CFD Model	The simplicity of these models allows the study of physical parameters associated with fluids such as pressure, velocity and temperature with adequate numerical accuracy.	Two-dimensional solution restricts the possibility to analyse hydraulic parameters such as water and/or air-flow rate (in the case of pipes with air valves).
	A 2D CFD model shows the variations in physical quantities (pressure, temperature, velocity) at different points of the hydraulic system by means of contours.	Contractions and expansions in pipes must be adjusted by geometric aspect ratios to obtain a guarantee of equivalent mass flow [22,34].
	Allows the visualisation of physical phenomena associated with water and air-flows, such as (i) deformation of the air–water interface and (ii) backflow air [7,20].	Simulations require more computational resources in comparison with mathematical models.
	The effect of opening drain valves can be simulated by means of a dynamic mesh [21].	
	On multi-core processors, simulation times are significantly reduced.	
3D CFD Model	The 3D CFD models show complete information on the physical, hydraulic and thermodynamic phenomena associated with transient flows in pipes with entrapped air during emptying events, simulating real conditions.	The definition of mesh quality, boundary conditions and numerical schemes are more difficult to calibrate, and require an independent analysis of the numerical results on the spatial discretisation conditions.
	In addition to the backflow air and the deformation of the air–water interface, this model allows obtaining new information such as (i) water flow rates, (ii) transient flows in the pipe cross-sectional, (iii) velocity profiles in different planes, (iv) heat transfer between water and air and (v) analysis of flow parameters with contour view in cross-sections [8,24].	Simulation times on high-performance processors are on the order of hours or days.
	The simulation of the drain valve approximates the real conditions in more detail.	These models require more significant computational resources than the other models.

5. Conclusions

Transient flows during emptying processes in pipelines with trapped air correspond to a topic in pipeline hydraulics, where phenomena such as water hammer and cavitation have been studied in detail considering a single-phase flow (water). Two-phase transient flows in emptying processes continue to be a subject under study. Currently, mathematical models have been developed in the literature, which have been experimentally validated. Mathematical models offer numerical information of interest such as water drainage velocity, air pocket pressure patterns, water flow rate, air admission flow rate (in cases of pipes with air valves installed) and temperature patterns. Mathematical models have been characterised by their simplicity in solving pipe hydraulics problems involving entrapped air. However, engineering projects in certain scenarios require more information on phenomena that are not captured by simple models available in the literature. Computational fluid dynamics

has been used to explore and study different hydraulic and thermodynamic phenomena that occur in pipelines during an emptying process with air entrapped. To this end, 2D and 3D CFD models were developed by different authors to represent emptying processes in pressurised pipelines with trapped air. CFD models provide useful and relevant numerical results for a detailed analysis of hydraulic phenomena resulting from air–water interaction during transient events in pressurised pipelines, such as (i) deformation and real-time location of the air–water interface, (ii) velocity contours, (iii) backflow air intrusion, (iv) air pocket pressure patterns as well as water flow patterns at different points in the pipes and (v) heat transfer between water and air. Based on the development of mathematical and CFD models, the following items can be concluded:

- Mathematical models based on the rigid column model are a fundamental tool for understanding the physical evolution of several hydraulic and thermodynamic variables based on differential equations that can be manipulated by the user according to the hydraulic scenario that is to be studied. These models have been validated in different investigations, showing good agreement with experimental measurements, and, additionally, they have been applied in large-scale hydraulic scenarios [19,36];
- A 2D CFD model allows study of the emptying process of an irregular pipeline with an air valve. The presence of air valves facilitates the air admission process during the water drainage process and mitigates subatmospheric pressures. In this sense, 2D CFD models are suitable for a simplified analysis of the interaction between air and water, with acceptable numerical and spatial resolution. The use of 2D CFD models is useful in cases where numerical information associated with physical parameters, such as velocity, pressure and heat transfer at different points of the pipeline, and visual information about the interaction between air and water are needed. These models require less computational time than a 3D CFD model and must be used with restrictions for the study of the emptying of pipes with air valves, when section changes occur (contractions, reductions), with the purpose of adjusting the mass flow conditions by means of a geometric aspect ratio defined in the literature for the sizing of orifices in pipes;
- A 3D CFD model allows simulation of the drainage of a single pipe in two cases (without air valves and with air valves). In Case 1, adverse subatmospheric pressures are generated due to entrapped air pockets and water flow oscillations. On the other hand, in Case 2, fewer critical pressure oscillations are observed compared to Case 1, due to the influence of the air admission orifices. All CFD model results in both cases were compared with the patterns recorded by the mathematical model, generally proposed by Fuertes-Miquel et al. [18]. It was observed that 3D CFD models showed hydraulic–thermodynamic phenomena that cannot be obtained in 2D CFD models, such as velocity distribution in pipe cross-sections, transient flows in pipe cross-sections, small air pockets created due to backflow air effect and their influence on water drainage flow transitions. In addition, there is the presence of a phenomenon that has not been studied in the literature, which is the temperature gradients between water and air phases, considering that the air pockets present a decrease in temperature due to the subatmospheric pressures and the water phase influences in heat transfer.

Future Research

The scientific literature presents several phenomena that have not yet been studied on the modelling of pressurised pipes with entrapped air using mathematical models and computational fluid dynamics. The calibration of mathematical and 2D/3D CFD models to study transient flows remains a challenge for researchers, considering the multiple hydraulic–thermodynamic phenomena that can occur due to the interaction between water and entrapped air pockets in pressurised pipes. In the last 5 years, 2D CFD models have been developed to study the emptying processes in pipelines, to study the backflow air effect and the influence of air valve sizing, obtaining good numerical results. Recently, the authors developed a 3D CFD model to study the emptying process of a pipe without

air valves, which is an important contribution to the literature. For future research, it is important to study the dynamic air–water interaction in large-scale water distribution networks using CFD models.

Therefore, CFD modelling is projected to be a tool that can be useful for its application at the engineering stage in the solution of hydraulic engineering problems involving air–water interaction in water distribution networks.

Author Contributions: Conceptualisation, D.A.P.-V. and O.E.C.-H.; methodology, D.A.P.-V.; software, D.A.P.-V. and H.G.E.-R.; validation, D.A.P.-V.; formal analysis, D.A.P.-V.; investigation, D.A.P.-V., O.E.C.-H. and H.G.E.-R.; resources, V.S.F.-M. and H.M.R.; writing—original draft preparation, D.A.P.-V.; writing—review and editing, D.A.P.-V. and O.E.C.-H.; visualisation, H.M.R. and V.S.F.-M.; supervision, H.M.R. and V.S.F.-M. All authors have read and agreed to the published version of the manuscript.

Funding: This research received no external funding.

Institutional Review Board Statement: Not applicable.

Informed Consent Statement: Not applicable.

Data Availability Statement: Not applicable.

Conflicts of Interest: The authors declare no conflict of interest.

Notation

The following notations are used in this manuscript:

A	pipe cross section (m^2)
C_{adm}	admission coefficient (–)
d_{adm}	admission orifice diameter (m)
$D_{k/\omega}$	diffusivity terms for k and/or ω (m^2/s)
e	specific energy (J/kg)
f	friction factor (–)
F_s	surface tension (kg/s^2)
g	gravitational acceleration (m/s^2)
$\mathbf{g}$	gravitational acceleration vector (m/s)
k	turbulent kinetic energy (m^2/s^2)
L_{iap}	initial air pocket length (m)
L_{ap}	air pocket length (m)
L_e	water column length (m)
m	mass (kg)
p	static pressure (N/m^2)
$\mathbf{q}$	heat flux vector (w/m^2)
Q	flow rate (m^3/s)
R_e	Reynolds number (–)
R_v	ball valve resistance coefficient ($m\ s^2/m^6$)
R	universal gas constant ($kg{\cdot}m^2s^{-2}K^{-1}mol^{-1}$)
$S_{k/\omega}$	source term of k or ω
T	temperature (°C)
t_m	ball valve opening time (s)
t	time (s)
u	velocity (m/s)
$\mathbf{u}$	velocity vector (m/s)
u_r	velocity source (m/s)
u_e	water column velocity (mathematical model) (m/s)
V	volume (m^3)
α_w	phase fraction of water (–)
κ	polytropic coefficient (–)
μ	dynamic viscosity (kg/(ms)

ν	kinematic viscosity (kg/ms)
ρ	density (kg/m^3)
ϕ	inner pipe diameter (m)
τ	ball valve opening degree (%)
ω	dissipation frequency (s^{-1})

Subscripts

a	refers to air phase (e.g., air density)
adm	refers to air admission orifice (e.g., cross section of air admission orifice)
atm	refers to atmospheric conditions (e.g., atmospheric pressure)
nc	refers to normal conditions (e.g., air density in normal conditions)
w	refers to water phase (e.g., water density)

SST k–ω coefficients

$CD_{k\omega}$	closure coefficient of k and ω
γ	refers to air phase (e.g., air density)
β	mass and energy transfer constant
β^*	turbulence transport constant

References

1. Chosie, C.D.; Hatcher, T.M.; Vasconcelos, J.G. Experimental and numerical investigation on the motion of discrete air pockets in pressurized water flows. *J. Hydraul. Eng.* **2014**, *140*, 04014038. [CrossRef]
2. AWWA. *Air Release, Air/Vacuum Valves and Combination Air Valves (M51)*; American Water Works Association: Denver, CO, USA, 2016.
3. Lauchlan, C.; Escarameia, M.; May, R.; Burrows, R.; Gahan, C. *Air in Pipelines—A Literature Review*; Report SR; HR Wallingford: Wallingford, UK, 2005; Volume 649.
4. Martin, C.S. Entrapped air in pipelines. In Proceedings of the Second International Conference on Pressure Surges, London, UK, 22–24 September 1976.
5. Fuertes-Miquel, V.S.; Coronado-Hernández, O.E.; Mora-Meliá, D.; Iglesias-Rey, P.L. Hydraulic modeling during filling and emptying processes in pressurized pipelines: A literature review. *Urban Water J.* **2019**, *16*, 299–311. [CrossRef]
6. Coronado Hernández, Ó.E. Transient Phenomena during the Emptying Process of Water in Pressurized Pipelines. Ph.D. Thesis, Universitat Politècnica de València, Valencia, Spain, 2019.
7. Besharat, M.; Coronado-Hernández, O.E.; Fuertes-Miquel, V.S.; Viseu, M.T.; Ramos, H.M. Computational fluid dynamics for sub-atmospheric pressure analysis in pipe drainage. *J. Hydraul. Res.* **2019**, *58*, 553–565. [CrossRef]
8. Paternina-Verona, D.A.; Coronado-Hernández, O.E.; Aguirre-Mendoza, A.M.; Espinoza-Román, H.G.; Fuertes-Miquel, V.S. Three-dimensional simulation of transient flows during the emptying of pipes with entrapped air. *J. Hydraul. Eng.* **2023**, *149*, 04023007. [CrossRef]
9. Fuertes, V. Hydraulic Transients with Entrapped Air Pockets. Ph.D. Thesis, Department of Hydraulic Engineering, Polytechnic University of Valencia, Editorial Universitat Politècnica de València, Valencia, Spain, 2001.
10. Zhou, L.; Liu, D.; Karney, B. Investigation of hydraulic transients of two entrapped air pockets in a water pipeline. *J. Hydraul. Eng.* **2013**, *139*, 949–959. [CrossRef]
11. Zhou, L.; Liu, D.; Karney, B.; Wang, P. Phenomenon of white mist in pipelines rapidly filling with water with entrapped air pockets. *J. Hydraul. Eng.* **2013**, *139*, 1041–1051. [CrossRef]
12. Zhou, L.; Pan, T.; Wang, H.; Liu, D.; Wang, P. Rapid air expulsion through an orifice in a vertical water pipe. *J. Hydraul. Res.* **2019**, *57*, 307–317. [CrossRef]
13. Zhou, L.; Lu, Y.; Karney, B.; Wu, G.; Elong, A.; Huang, K. Energy dissipation in a rapid filling vertical pipe with trapped air. *J. Hydraul. Res.* **2023**, *61*, 120–132. [CrossRef]
14. Laanearu, J.; Annus, I.; Koppel, T.; Bergant, A.; Vučković, S.; Hou, Q.; Tijsseling, A.S.; Anderson, A.; van't Westende, J.M. Emptying of large-scale pipeline by pressurized air. *J. Hydraul. Eng.* **2012**, *138*, 1090–1100. [CrossRef]
15. Laanearu, J.; Hou, Q.; Annus, I.; Tijsseling, A.S. Water-column mass losses during the emptying of a large-scale pipeline by pressurized air. *Proc. Est. Acad. Sci.* **2015**, *64*, 8. [CrossRef]
16. Tijsseling, A.S.; Hou, Q.; Bozkuş, Z.; Laanearu, J. Improved one-dimensional models for rapid emptying and filling of pipelines. *J. Press. Vessel Technol.* **2016**, *138*, 031301. [CrossRef]
17. Coronado-Hernández, O.E.; Fuertes-Miquel, V.S.; Besharat, M.; Ramos, H.M. Experimental and Numerical Analysis of a Water Emptying Pipeline Using Different Air Valves. *Water* **2017**, *9*, 98. [CrossRef]
18. Fuertes-Miquel, V.S.; Coronado-Hernández, O.E.; Iglesias-Rey, P.L.; Mora-Meliá, D. Transient phenomena during the emptying process of a single pipe with water–air interaction. *J. Hydraul. Res.* **2019**, *57*, 318–326. [CrossRef]

19. Romero, G.; Fuertes-Miquel, V.S.; Coronado-Hernández, Ó.E.; Ponz-Carcelén, R.; Biel-Sanchis, F. Analysis of hydraulic transients during pipeline filling processes with air valves in large-scale installations. *Urban Water J.* **2020**, *17*, 568–575. [CrossRef]
20. Besharat, M.; Coronado-Hernández, O.E.; Fuertes-Miquel, V.S.; Viseu, M.T.; Ramos, H.M. Backflow air and pressure analysis in emptying a pipeline containing an entrapped air pocket. *Urban Water J.* **2018**, *15*, 769–779. [CrossRef]
21. Hurtado-Misal, A.D.; Hernández-Sanjuan, D.; Coronado-Hernández, O.E.; Espinoza-Román, H.; Fuertes-Miquel, V.S. Analysis of Sub-Atmospheric Pressures during Emptying of an Irregular Pipeline without an Air Valve Using a 2D CFD Model. *Water* **2021**, *13*, 2526. [CrossRef]
22. Paternina-Verona, D.A.; Coronado-Hernández, O.E.; Fuertes-Miquel, V.S. Numerical modelling for analysing drainage in irregular profile pipes using OpenFOAM. *Urban Water J.* **2022**, *19*, 569–578. [CrossRef]
23. Paternina-Verona, D.A.; Flórez-Acero, L.C.; Coronado-Hernández, O.E.; Espinoza-Román, H.G.; Fuertes-Miquel, V.S.; Ramos, H.M. Two-dimensional simulation of emptying manoeuvres in water pipelines with admitted air. *Urban Water J.* **2023**, *20*, 1–12. [CrossRef]
24. Paternina-Verona, D.A.; Coronado-Hernández, O.E.; Espinoza-Román, H.G.; Besharat, M.; Fuertes-Miquel, V.S.; Ramos, H.M. Three-Dimensional Analysis of Air-Admission Orifices in Pipelines during Hydraulic Drainage Events. *Sustainability* **2022**, *14*, 14600. [CrossRef]
25. Paternina-Verona, D.A.; Coronado-Hernández, O.E.; Espinoza-Román, H.G.; Fuertes-Miquel, V.S.; Ramos, H.M. Rapid Filling Analysis with an Entrapped Air Pocket in Water Pipelines Using a 3D CFD Model. *Water* **2023**, *15*, 834. [CrossRef]
26. Greenshields, C.; Weller, H. *Notes on Computational Fluid Dynamics: General Principles*; CFD Direct Ltd.: Reading, UK, 2022.
27. Hirt, C.W.; Nichols, B.D. Volume of Fluid (VOF) method for the dynamics of free boundaries. *J. Comput. Phys.* **1981**, *39*, 201–225. [CrossRef]
28. Bombardelli, F.A.; Hirt, C.; García, M.H.; Matthews, B.; Fletcher, C.; Partridge, A.; Vasquez, S. Computations of curved free surface water flow on spiral concentrators. *J. Hydraul. Eng.* **2001**, *127*, 629–631. [CrossRef]
29. Menter, F.R. Two-equation eddy-viscosity turbulence models for engineering applications. *AIAA J.* **1994**, *32*, 1598–1605. [CrossRef]
30. Menter, F.R. Review of the shear-stress transport turbulence model experience from an industrial perspective. *Int. J. Comput. Fluid Dyn.* **2009**, *23*, 305–316. [CrossRef]
31. Menter, F.; Esch, T. Elements of industrial heat transfer predictions. In Proceedings of the 16th Brazilian Congress of Mechanical Engineering (COBEM), Uberlandia, Brazil, 26–30 November 2001; Volume 109, p. 650.
32. Huang, B.; Fan, M.; Liu, J.; Zhu, D.Z. CFD Simulation of Air–Water Interactions in Rapidly Filling Horizontal Pipe with Entrapped Air. In Proceedings of the World Environmental and Water Resources Congress 2021, Virtually, 7–11 June 2021; pp. 495–507.
33. Zhou, L.; Wang, H.; Karney, B.; Liu, D.; Wang, P.; Guo, S. Dynamic behavior of entrapped air pocket in a water filling pipeline. *J. Hydraul. Eng.* **2018**, *144*, 04018045. [CrossRef]
34. Aguirre-Mendoza, A.M.; Oyuela, S.; Espinoza-Román, H.G.; Coronado-Hernández, O.E.; Fuertes-Miquel, V.S.; Paternina-Verona, D.A. 2D CFD Modeling of Rapid Water Filling with Air Valves Using OpenFOAM. *Water* **2021**, *13*, 3104. [CrossRef]
35. Aguirre-Mendoza, A.M.; Paternina-Verona, D.A.; Oyuela, S.; Coronado-Hernández, O.E.; Besharat, M.; Fuertes-Miquel, V.S.; Iglesias-Rey, P.L.; Ramos, H.M. Effects of Orifice Sizes for Uncontrolled Filling Processes in Water Pipelines. *Water* **2022**, *14*, 888. [CrossRef]
36. Romero, G.; Fuertes-Miquel, V.S.; Coronado-Hernández, Ó.E.; Ponz-Carcelén, R.; Biel-Sanchis, F. Transient phenomena generated in emptying operations in large-scale hydraulic pipelines. *Water* **2020**, *12*, 2313. [CrossRef]
37. Zhou, L.; Liu, D.Y.; Ou, C.Q. Simulation of flow transients in a water filling pipe containing entrapped air pocket with VOF model. *Eng. Appl. Comput. Fluid Mech.* **2011**, *5*, 127–140. [CrossRef]
38. Martins, N.M.; Delgado, J.N.; Ramos, H.M.; Covas, D.I. Maximum transient pressures in a rapidly filling pipeline with entrapped air using a CFD model. *J. Hydraul. Res.* **2017**, *55*, 506–519. [CrossRef]